Supporting Information

Multi-Modal Control Over the Assembly of a Molecular Motor in Water

Fan Xu, Lukas Pfeifer, Marc C. A. Stuart, Franco King-Chi Leung,* Ben L. Feringa*

Stratingh Institute for Chemistry, University of Groningen Nijenborgh 4, 9747 AG, Groningen, Netherlands. E-mail: b.l.feringa@rug.nl, kingchifranco.leung@polyu.edu.hk
(Present address of Franco King-Chi Leung: State Key Laboratory of Chemical Biology & Drug Discovery, Department of Applied Biology and Chemical Technology, The Hong Kong Polytechnic University, Hong Kong, China)

Table of Contents

1. Materials. All commercial reagents were purchased from Acros, Aldrich, TCI or Merck and were used as received. All solvents used in the reactions were dried using an MBraun SPS-800 solvent purification system or purchased from Acros, except for MeOH. Analytical TLC was performed on Merck silica gel 60 F254 plates and visualization was accomplished by UV light. Solvents for spectroscopic studies were of spectrophotometric grade (UVASOL Merck). Aq. stock solutions (0.1 M) of NaOH and HCl were prepared freshly using Milli-Q water. Nile Red stock solution (1.0×10^{-3} M) was prepared in EtOH.

2. General. Column chromatography was performed on a Reveleris X2 Flash Chromatography system. NMR spectra were recorded at 25 °C on Varian AMX400 or Agilent 400-MR (^{1}H: 400 MHz, ^{13}C: 101 MHz) spectrometers. Chemical shifts (δ) are expressed relative to the resonances of the residual non-deuterated solvent for ^{1}H [$CDCl_3$: ^{1}H(δ) = 7.26 ppm] and ^{13}C [$CDCl_3$: ^{13}C(δ) = 77.0 ppm].. Absolute values of the coupling constants are given in Hertz (Hz), regardless of their sign. Multiplicities are abbreviated as singlet (s), doublet (d), doublet of doublets (dd), triplet (t), triplet of doublets (td), quartet (q), multiplet (m), and broad (br). High-resolution mass spectrometry (HRMS) was performed on an LTQ Orbitrap XL spectrometer with ESI ionization. All reactions were performed under anhydrous conditions under a N_2 atmosphere.

3. Synthesis of MBA.

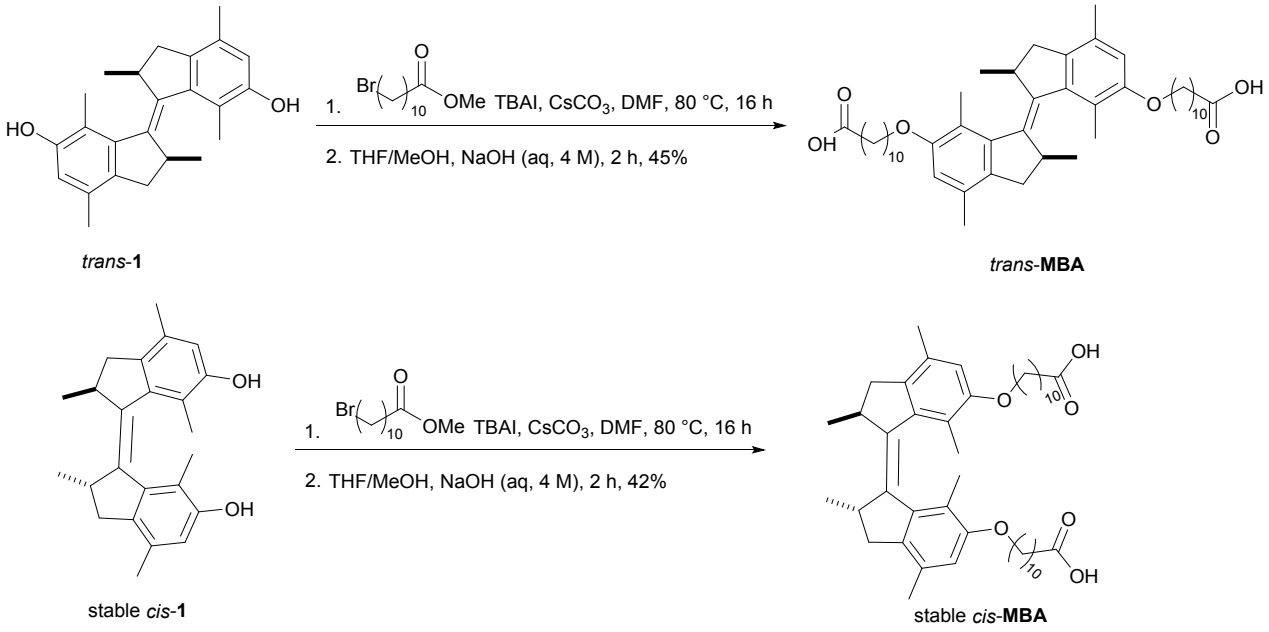

Scheme S1 Synthesis of *trans*-**MBA** and stable *cis*-**MBA**

3.1 Compound 1.
Trans-**1** and stable *cis*-**1** were synthesized following our group's published method.[1,2]

3.2 *Trans*-MBA.
A solution of *trans*-**1** (100 mg, 0.287 mmol) in DMF (2 mL) was added to methyl-11-bromoundecanoate (321 mg, 1.15 mmol), tetrabutylammonium iodide (414 mg, 1.15 mmol) and Cs_2CO_3 (374 mg, 1.15 mmol), and the reaction mixture was stirred at 80 °C for 16 h. De-ionized (DI) water (15 mL) was added and the aqueous phase was extracted with EtOAc (3 × 15 mL). The combined organic phases were dried over Na_2SO_4 and concentrated *in vacuo*. The crude product was purified by flash column chromatography (SiO_2, pentane/EtOAc 19/1) to afford the corresponding ester as a colorless oil. To a

solution of aq. NaOH (0.3 mL, 4 M), THF (3 mL) and MeOH (3 mL) was added the ester. The reaction mixture was heated at reflux for 2 h then concentrated *in vacuo*. DI water (10 mL) and aq. HCl (1 M) was added to adjust pH < 7. The aqueous phase was extracted with EtOAc (3 × 10 mL). The combined organic layers were washed with brine (30 mL), dried over Na_2SO_4 and concentrated *in vacuo*. The crude product was purified by column chromatography (SiO_2, pentane/EtOAc 8/2) to afford *trans*-**MBA** as a colourless solid. (93 mg, 0.13 mmol, 45%)

^{1}H NMR (400 MHz, $CDCl_3$) δ 6.54 (s, 2H), 4.03 – 3.90 (m, 4H), 2.89 (p, J = 6.3 Hz, 2H), 2.59 (dd, J = 14.1, 5.6 Hz, 2H), 2.39 – 2.28 (m, 10H), 2.20 – 2.11 (m, 8H), 1.87 – 1.78 (m, 4H), 1.63 (m, 4H), 1.51 (m, 4H), 1.36 – 1.26 (m, 20H), 1.09 (d, J = 6.4 Hz, 6H).

^{13}C NMR (101 MHz, $CDCl_3$) δ 180.0, 156.6, 142.7, 142.0, 134.1, 131.4, 120.8, 111.2, 68.7, 42.5, 38.7, 34.3, 29.9, 29.8, 29.7, 29.7, 29.5, 29.4, 26.6, 25.0, 19.5, 19.0, 16.5.

HRMS (FTMS – n ESI) found $[M\text{-}H]^-$, calculated: 715.49431; found: 715.49701.

3.3 Stable *cis*-MBA.

Stable *cis*-**MBA** was synthesized from stable *cis*-**1** by using the same method and scale as described for *trans*-**MBA** in section 3.2. The crude product was purified by flash column chromatography (SiO_2, pentane/EtOAc 8/2) to afford stable *cis*-**MBA** as a colourless solid. (87 mg, 0.12 mmol, 42%)

^{1}H NMR (400 MHz, $CDCl_3$) δ 6.53 (s, 2H), 3.96 – 3.80 (m, 4H), 3.32 (p, J = 6.7 Hz, 2H), 3.03 (dd, J = 14.5, 6.3 Hz, 2H), 2.40 – 2.29 (m, 6H), 2.24 (s, 6H), 1.73 (m, 4H), 1.63 (m, 4H), 1.50 – 1.24 (m, 30H), 1.07 (d, J = 6.7 Hz, 6H).

^{13}C NMR (400 MHz, $CDCl_3$) δ 179.6, 155.6, 141.8, 140.6, 135.6, 130.0, 122.2, 111.5, 68.4, 41.5, 37.7, 33.7, 29.3, 29.0, 29.0, 28.9, 28.7, 28.5, 25.7, 24.3, 20.2, 18.5, 14.0.

HRMS (FTMS – n ESI) $[M\text{-}H]^-$, calculated: 715.49431; found: 715.49454.

4. Photochemistry Experiments.

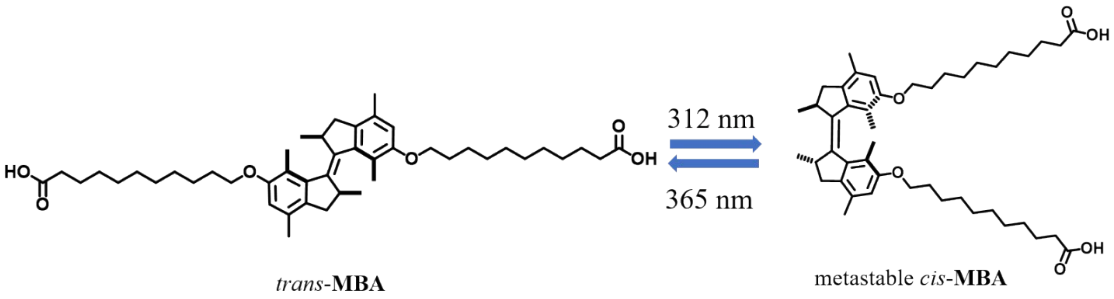

trans-**MBA** metastable *cis*-**MBA**

The photo-responsive behaviour was studied by steady-state absorption and ^{1}H NMR spectroscopy. CD_3OD and MeOH were degassed by bubbling argon for 30 min prior to use in the photoisomerization experiments followed by NMR and UV-vis absorption spectrometry. UV-vis spectra were recorded on a Hewlet-Packard HP 8543 Diode Array in a 1 cm path length quartz cuvette. Irradiation of *trans*-**MBA** in degassed MeOH were carried out at 25 °C using a Spectroline hand-held UV lamp with LONGLIFE™ filter (8-watt model) positioned at a distance of 5 cm from the sample.

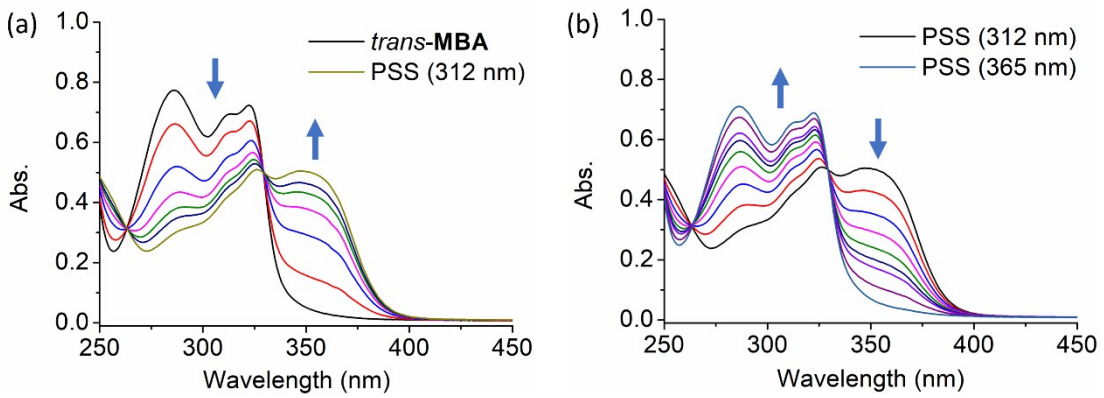

Fig. S1 Changes in UV/Vis absorption spectrum (a) over the course of irradiating a sample (1.0 x 10^{-5} M in degassed MeOH) of *trans*-**MBA** to PSS at 25 °C using 312 nm light and (b) during subsequent irradiation to PSS with 365 nm light.

5. Nile Red Fluorescence Assay.[3,4]

A stock solution of Nile Red (1.0×10^{-3} M in EtOH) was diluted with *trans*-**MBA** and stable *cis*-**MBA** solutions to a final concentration of 2.5×10^{-2} nM. Concentrations of *trans*-**MBA** and stable *cis*-**MBA** were ranging from 1.4×10^{-7} to 2.8×10^{-3} M. Sample solutions were excited at 550 nm wavelength and the emission spectra were recorded from 580–750 nm by using a JASCO FP6200 spectrofluorometer. Blue shifts were calculated by subtracting the emission wavelength of Nile Red in Milli-Q water from the emission wavelength of the samples. Blue shifts were plotted against **MBA** concentrations to determine critical aggregation concentrations. The results revealed CACs of 4.0×10^{-6} M and 1.0×10^{-5} M for *trans*-**MBA** and stable *cis*-**MBA** (Fig.S3).

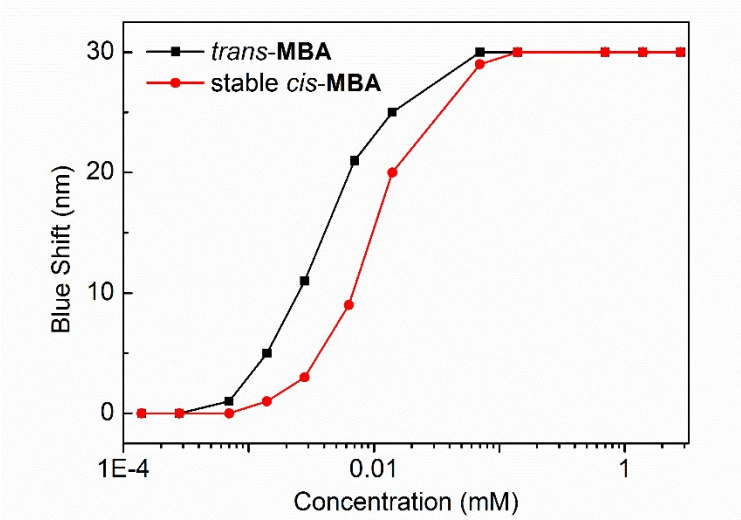

Fig. S2 Nile Red fluorescence assays for determination of the critical aggregation concentrations (CAC) of *trans*-**MBA** and stable *cis*-**MBA** (concentration: 1.4×10^{-7}–2.8×10^{-3} M).

To determine the counter-ion effect on the assembly of *trans*-**MBA**, Nile red fluorescence assay was employed to analyse aq. solutions containing *trans*-**MBA** (5.0×10^{-6} M), Nile red (2.5×10^{-11} M), and various metal chlorides (1.0×10^{-6}–5.0×10^{-1} M). Emission spectra were recorded and blue shifts calculated using the same method described in the last paragraph. Blue shifts were plotted against concentrations of metal chlorides.

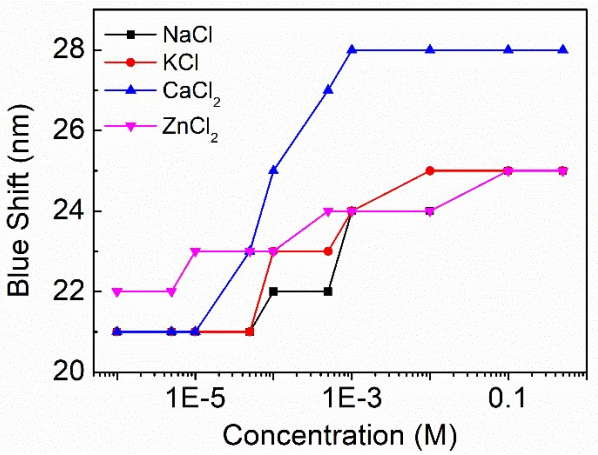

Fig. S3 Blue shift of Nile Red in *trans*-**MBA** solutions (5.0×10^{-6} M) containing various concentrations (1.0×10^{-6}–5.0×10^{-1} M) of NaCl, KCl, $CaCl_2$, and $ZnCl_2$.

6. Cryo-TEM Studies.

6.1 Sample Preparation.

In order to study the influence of irradiation on the assembly structure of **MBA** a dispersion of *trans*-**MBA** (7.0×10^{-3} M) in sodium borate buffer (pH = 9.3, 0.1 M) was heated at 80 °C for 30 min and then cooled down to room temperature to form ordered assemblies (Step 1). Then the solution was placed in a quartz cuvette (1 mm path length) and irradiated with 312 nm light for 10 min using a Spectroline hand-held UV lamp with LONGLIFE™ filter (8-watt model) (Step 2), followed by irradiation with 365 nm light for 10 min using the same lamp (Step 3). Finally, solutions after 312 nm and subsequent 365 nm irradiation were heated at 80 °C for 30 min and then cooled down to room temperature again (Step 4). 20 µL samples taken after each step were used for cryo-TEM measurements immediately. 100 µL solutions after Steps 1, 2 and 3 were freeze-dried and used in NMR studies (Fig. S4).

Solutions of stable *cis*-**MBA** used in cryo-TEM studies were prepared following the same method as described for *trans*-**MBA**. The self-assembly morphology of stable *cis*-**MBA** is shown in Fig. S1.

Assembly morphology transitions induced by pH were studied by adding varying amounts of an aq. NaOH stock solution (0.1 M) to an aq. solution of *trans*-**MBA** (7.0×10^{-3} M). Sample solutions at pH 8.8, pH 9.8 and pH 11 were heated at 80 °C for 30 min and cooled down to room temperature. A sample of pH 9.4 was prepared by adding an aq. HCl stock solution (0.1 M) to a sample solution of pH 11. The pH of the samples was determined using a Mettler-Toledo SevenEasy™ pH meter with Inlab hydrofluoric electrode.

In order to study the assembly morphology of *trans*-**MBA** as a function of the counter-ions, an aqueous dispersion of *trans*-**MBA** (7.0×10^{-3} M) with 2.0 equiv. of NaOH was heated at 80 °C for 30 min and cooled down to room temperature to afford the sample solution. An aq. NaCl (1.0 M) or $CaCl_2$ (5.0×10^{-2} M) stock solution was added to the sample solution to achieve the indicated chloride salts concentrations.

6.2 Characterization.

A few µL of each sample solution were placed on holey carbon coated copper grids (Quantifoil 3.5/1, Quantifoil Micro Tools, Jena, Germany). Grids with sample were vitrified in liquid ethane (Vitrobot, FEI, Eindhoven, The Netherlands) and transferred to a FEI T20 cryo-electron microscope equipped with a Gatan model 626 cryo-stage operating at 200 kV. Micrographs were recorded under low-dose conditions with a slow-scan CCD camera.

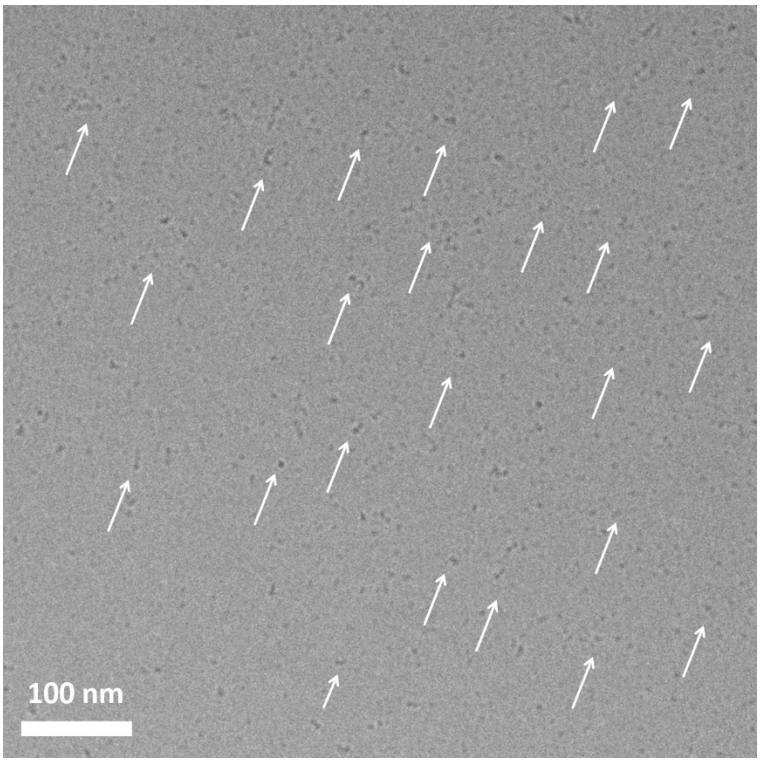

Fig. S4 Cryo-TEM image of stable *cis*-**MBA** (7.0×10^{-3} M) in sodium borate buffer (pH = 9.3, 0.1 M). (white arrows: micelles)

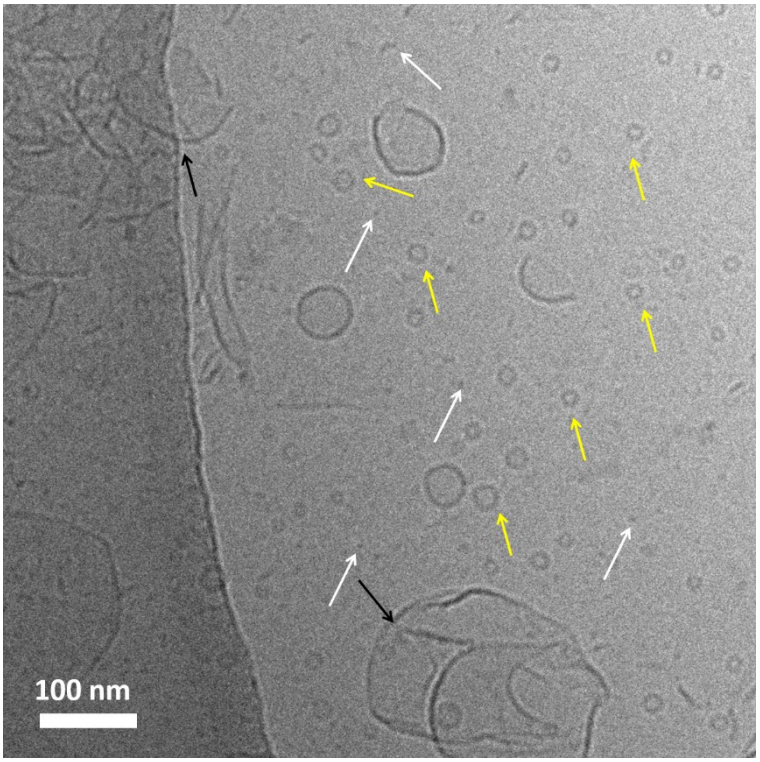

Fig. S5 Cryo-TEM image of *trans*-**MBA** (7.0×10^{-3} M) in sodium borate buffer (pH = 9.3, 0.1 M) after 312 nm irradiation for 10 min. (green: micelles, yellow: vesicles, black: sheets)

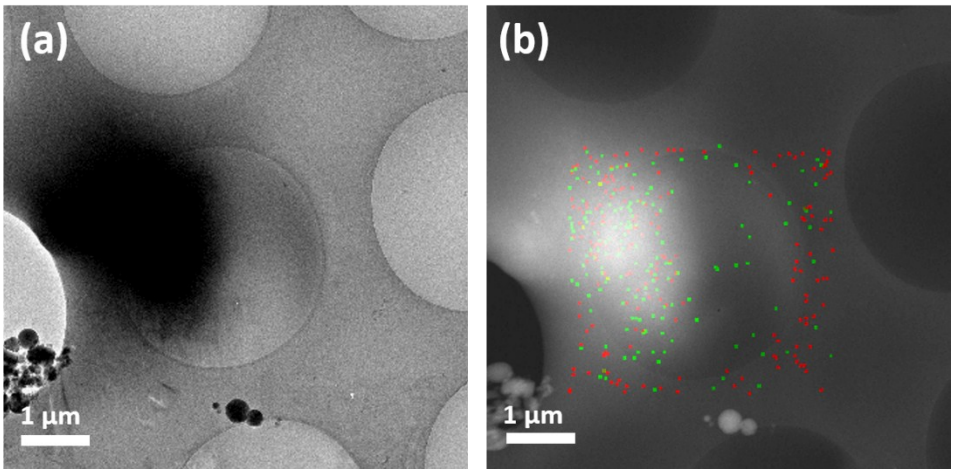

Fig. S6 (a) Cryo-TEM images of *trans*-**MBA** carboxylates (7.0×10^{-3} M) in 5.0×10^{-3} M $CaCl_2$ solution (b) elemental mapping of C (red) and Ca (green) of *trans*-**MBA** carboxylates at the same position.

Note on pH/Counter Ion Effect on Photoswitching

We performed the photoisomerization process on sample solutions of different pH = 8.8, 9.8, and 11. As shown in Fig. S7a, sheet-like aggregates were found in the solution of *trans*-**MBA** at pH 8.8. After 312 nm irradiation for 10 min, vesicles were observed as a mixture with the sheet-like assemblies (Fig. S7b). After subsequent photoirradiation with 365 nm light for 10 min, the sheet-like structures were reformed with some small vesicles remaining in the mixture (Fig. S7c). This was nearly identical to the result observed in sodium borate buffer. In addition, *trans*-**MBA** showed formation of disc-like structures in the sample solution at pH 9.8 (Fig. S7d). There was no significant morphological transformation observed after irradiating an identical sample with 312 nm light (Fig. S7e) and subsequent irradiation with 365 nm light (Fig. S7f). Furthermore, micellar structures were observed in the solution of *trans*-**MBA** at pH 11 (Fig. S7g), which showed no obvious assembly transformations following irradiation with 312 nm and 365 nm light (Fig. S7h–i).

Based on these studies, we determined that the self-assembly behaviour of **MBA** molecules is sensitive to pH variation. Photoisomerization induced assembly transformation was only observed in lower pH regimes (either pH 8.8 or sodium borate buffer with pH 9.3). However, at higher pH, **MBA** showed no significant morphological transformations upon irradiation.

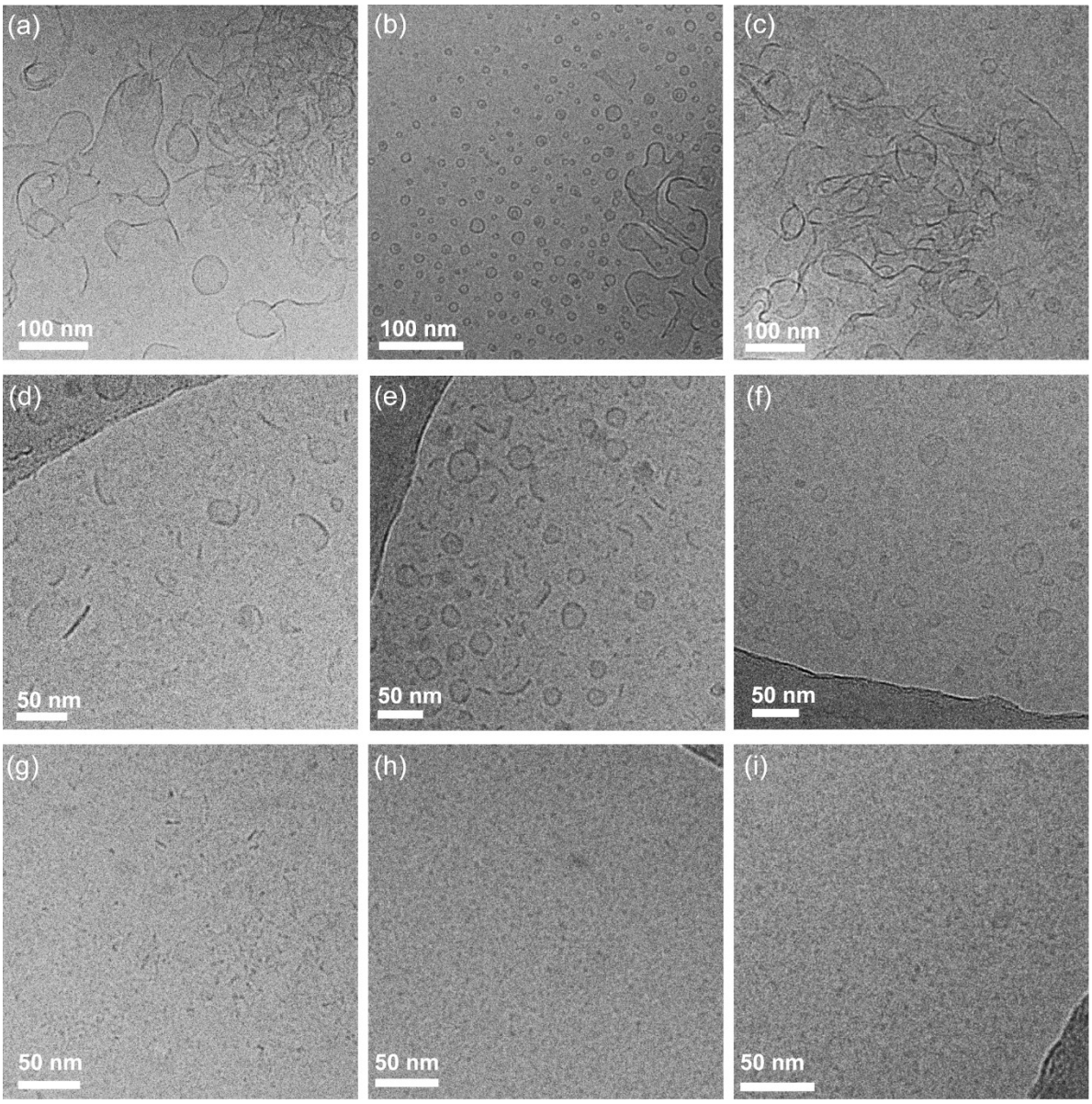

Fig. S7 Cryo-TEM images of *trans*-**MBA** (7 mM) in aq. NaOH solution with (a–c) pH = 8.8, (d–f) pH = 9.8, (g–i) pH = 11 (a,d,g) before and (b,e,h) after irradiation with 312 nm for 10 min, (c,f,i) as well as after subsequent 365 nm irradiation for 10 min, respectively.

Note on Potential Kinetically Locked State and Reversibility:

In the photoisomerization-induced assembly transformation, some vesicles remained unchanged after irradiation with 365 nm light which had also been observed in our previous work in 2016.[5] In both cases, it was possible to achieve complete reversal of the observed assembly state by subjecting the samples to a heating-cooling cycle. This can hint at the presence of kinetically locked states, however, this is not the main focus of this paper and we do not want to make this explicit claim.

With respect to the salt-induced change of assembly structure it has to be noted that reversibility of salt addition, has not been established in our presented method. As shown in the EDX data (Fig S6), metal ions are trapped in the aggregated structures and cannot be separated.

pH-dependent measurements: Upon addition of HCl (aq.) to a sample with pH 11 (Fig. 3) an immediate and complete change in assembly structure from micelles to vesicles was observed without need for a heating-cooling cycle. No indication for a kinetically locked state was therefore observed. The fact that the assembly structure was not reversed to the originally observed sheet-like assemblies, but that vesicles and congeries thereof were formed instead, is due to formation of NaCl accompanying the lowering of the sample pH as detailed in the main text.

7. NMR Spectra.

Note on ^{1}H NMR Characterization: The *cis*-*trans* ratio of **MBA** at the photostationary state (*cis*:*trans* = 63:37) was studied in deuterated methanol by ^{1}H NMR on a sample with a total concentration of 2.8 mM.(Fig. 1, S8) The molecules are dissolved very well in deuterated methanol, as suggested by the clear signals consisting of sharp peaks without line broadening in the obtained ^{1}H NMR spectra. Our measurements furthermore showed no CAC in deuterated methanol. On the other hand, it was not possible to obtain a clear spectrum of an identical sample in D_2O, because the concentration used for the ^{1}H NMR study was far beyond the CAC (4.0×10^{-3} mM) in aqueous medium.

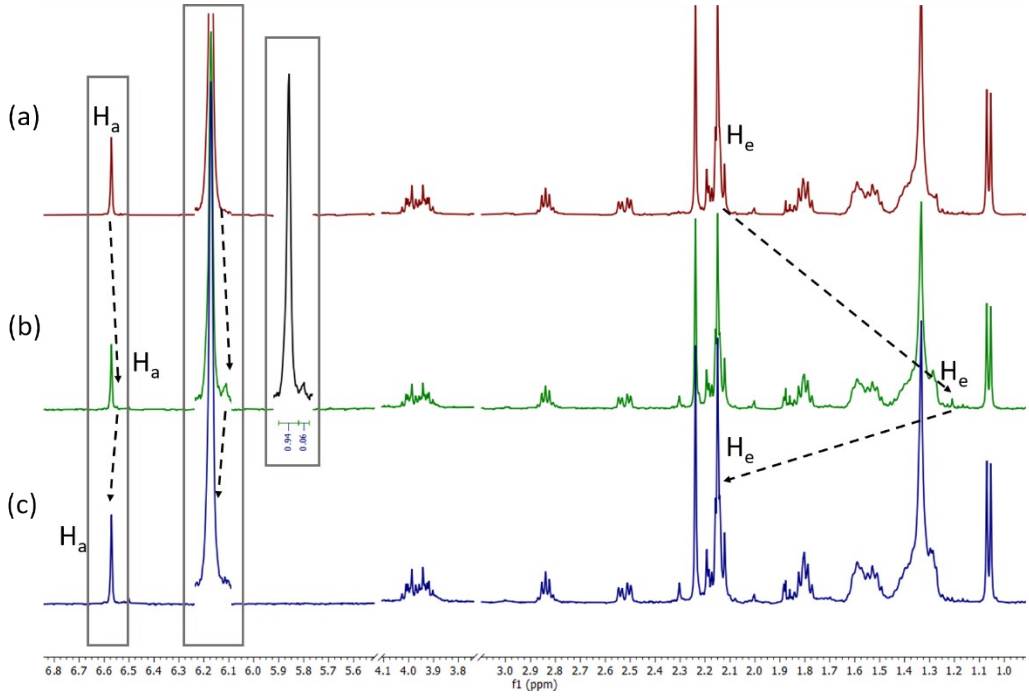

Fig. S8 ^{1}H NMR spectra (CD_3OD, 25 °C, 400 MHz) of freeze dried samples used in cryo-TEM studies: (a) *trans*-**MBA**, (b) mixture of *trans*-**MBA** and metastable *cis*-**MBA** obtained after irradiation with 312 nm light for 10 min in buffer (6% of metastable *cis*-**MBA** was calculated by integration) (c) after subsequent irradiation of the mixture with 365 nm light for 10 min. (Samples were freeze-dried before using in NMR studies, concentration in NMR study: 2.8×10^{-3} M)

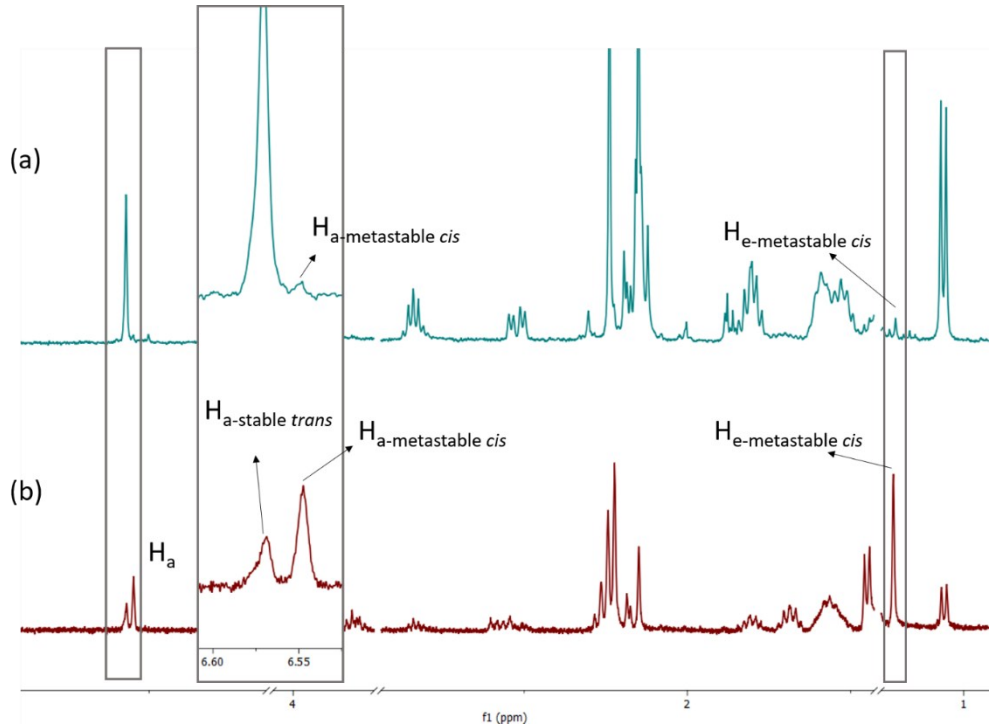

Fig. S9 ^{1}H NMR spectra (CD_3OD, 25 °C, 400 MHz) of (a) mixture of *trans*-**MBA** and metastable *cis*-**MBA** obtained after irradiation with 312 nm light for 10 min in buffer (Sample in buffer was freeze-dried before using in NMR studies.) (b) PSS_{312nm} mixture of metastable *cis*-**MBA** and *trans*-**MBA** with a ratio of 63:37 in MeOH. (concentration in NMR study: 2.8×10^{-3} M)

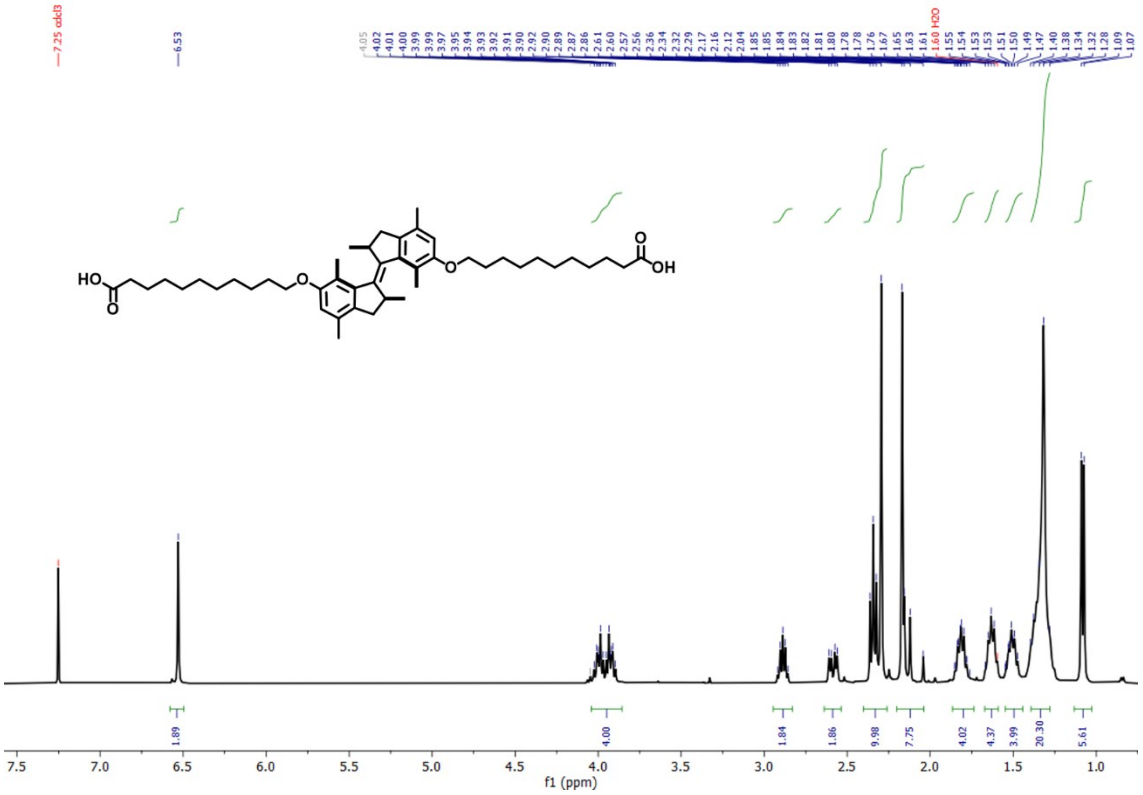

Fig. S10 ^{1}H NMR spectrum of *trans*-**MBA**. ($CDCl_3$, 25 °C, 400 MHz)

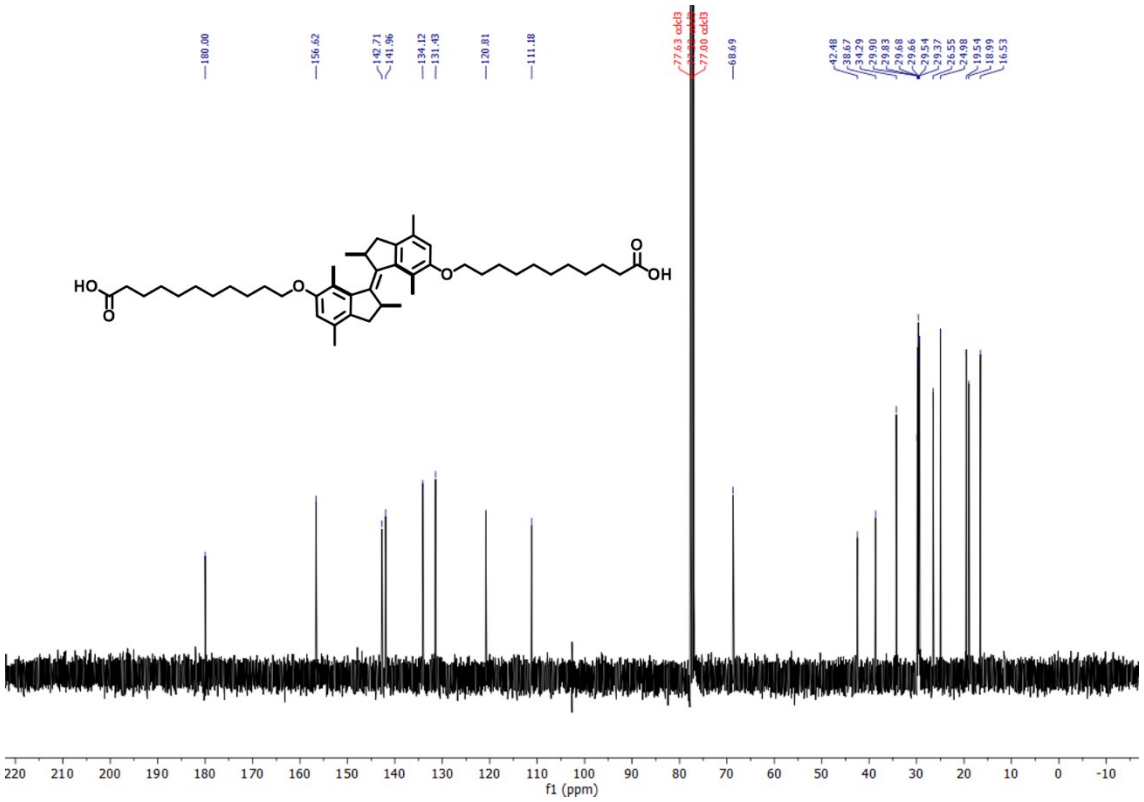

Fig. S11 ^{13}C NMR spectrum of *trans*-**MBA**. ($CDCl_3$, 25 °C, 101 MHz)

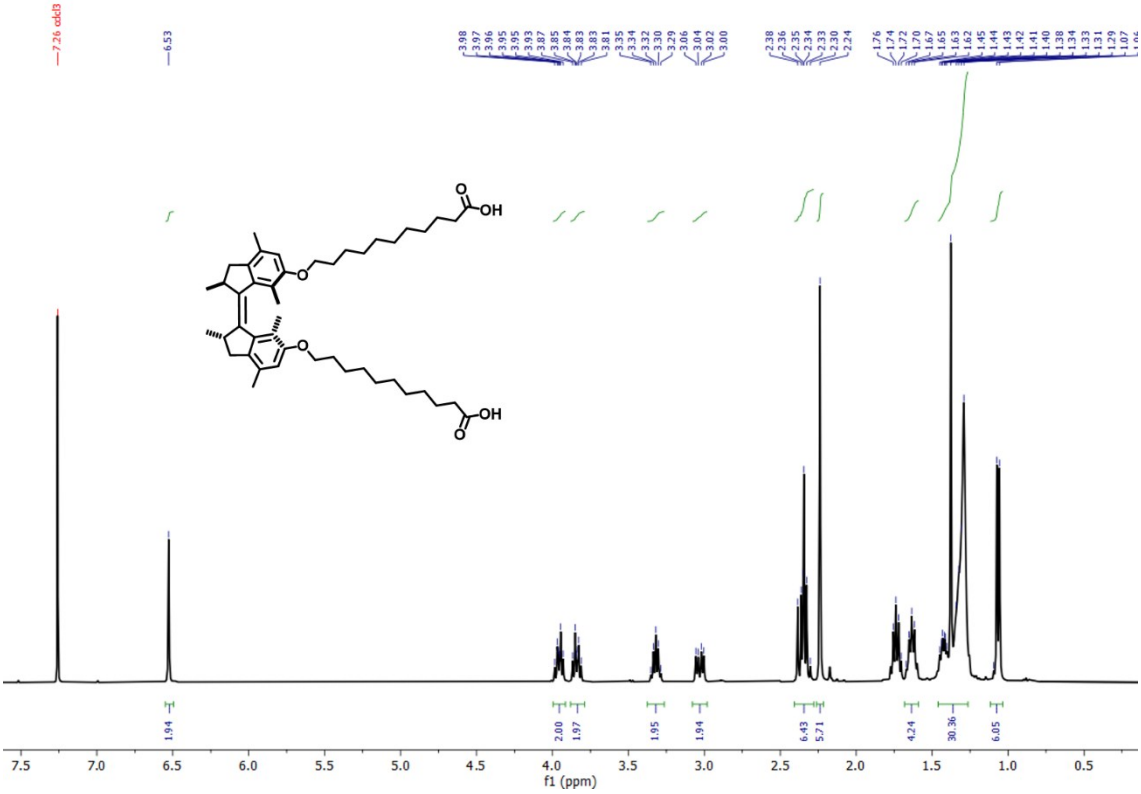

Fig. S12 ^{1}H NMR spectrum of stable *cis*-**MBA**. ($CDCl_3$, 25 °C, 400 MHz)

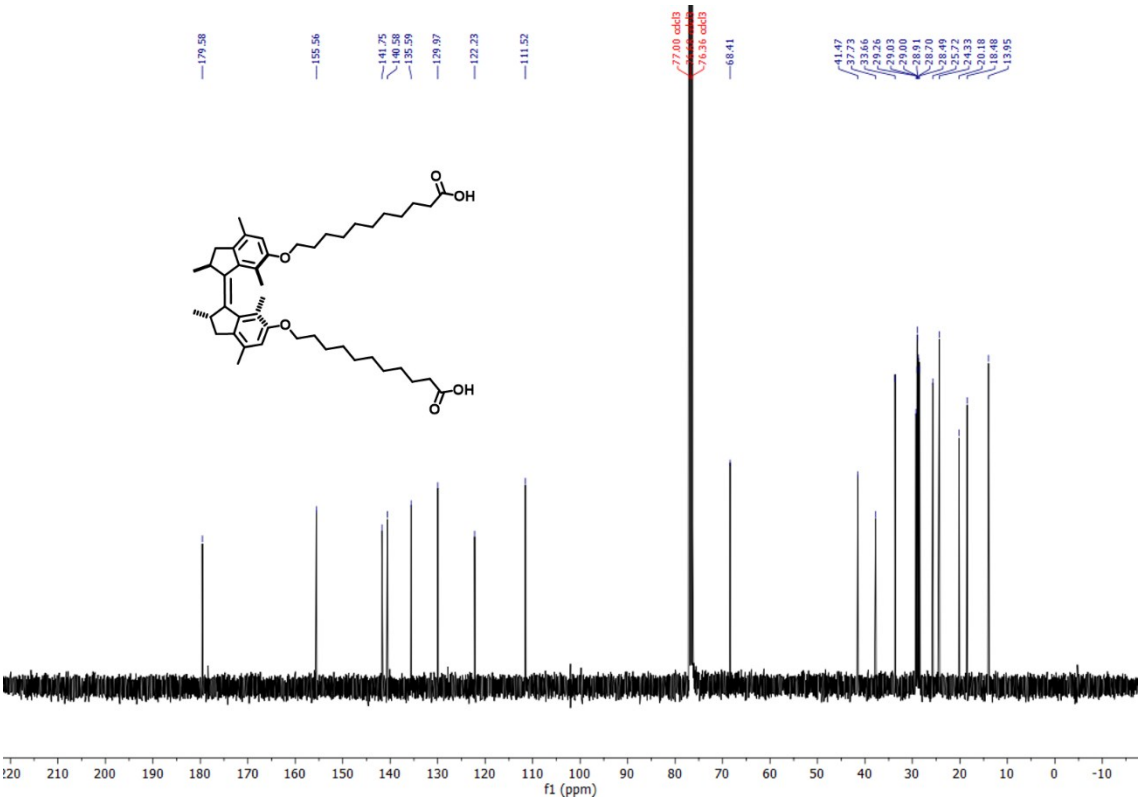

Fig. S13 ^{13}C NMR spectrum of stable *cis*-**MBA**. ($CDCl_3$, 25 °C, 101 MHz)

8. Wide-Field and Close-Up Cryo-TEM Images

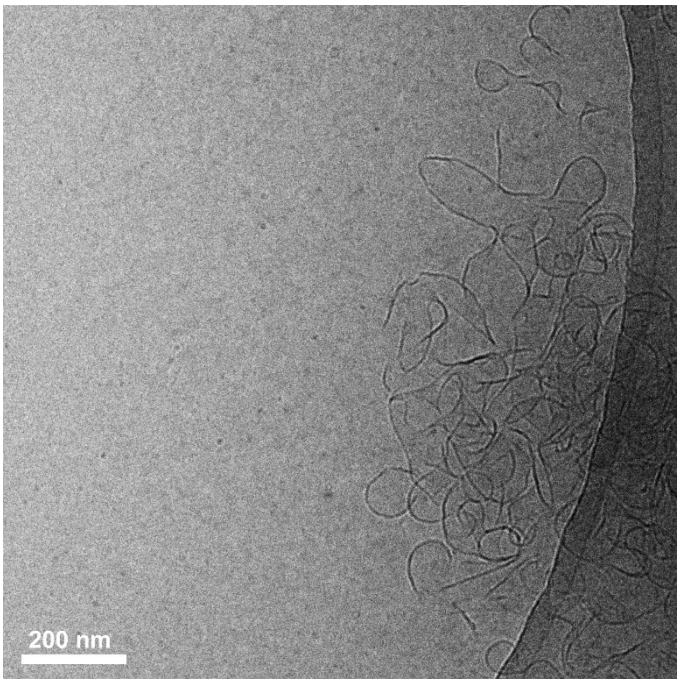

Fig. S14 Wide-field cryo-TEM image of *trans*-**MBA** (7.0×10^{-3} M) in sodium borate buffer (pH = 9.3, 0.1 M).

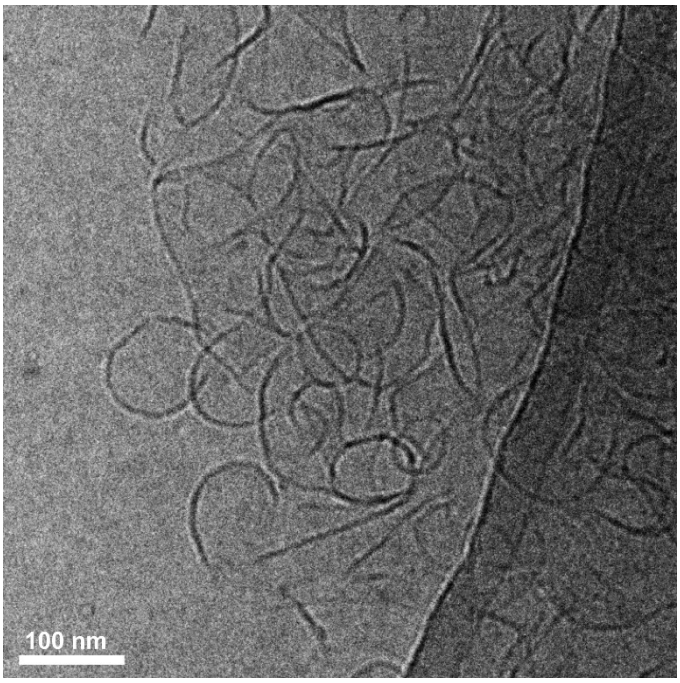

Fig. S15 Close-up cryo-TEM image of *trans*-**MBA** (7.0×10^{-3} M) in sodium borate buffer (pH = 9.3, 0.1 M).

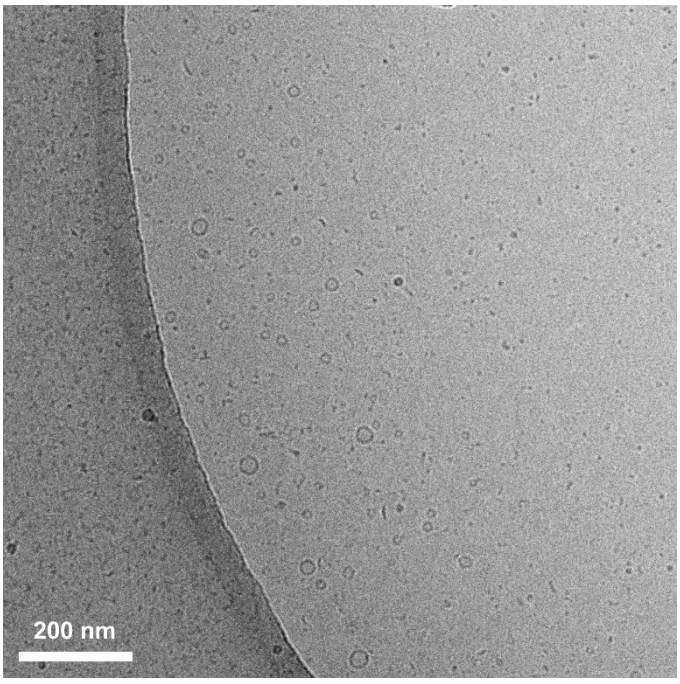

Fig. S16 Wide-field cryo-TEM image of *trans*-**MBA** (7.0×10^{-3} M) after irradiation with 312 nm for 10 min in sodium borate buffer (pH = 9.3, 0.1 M).

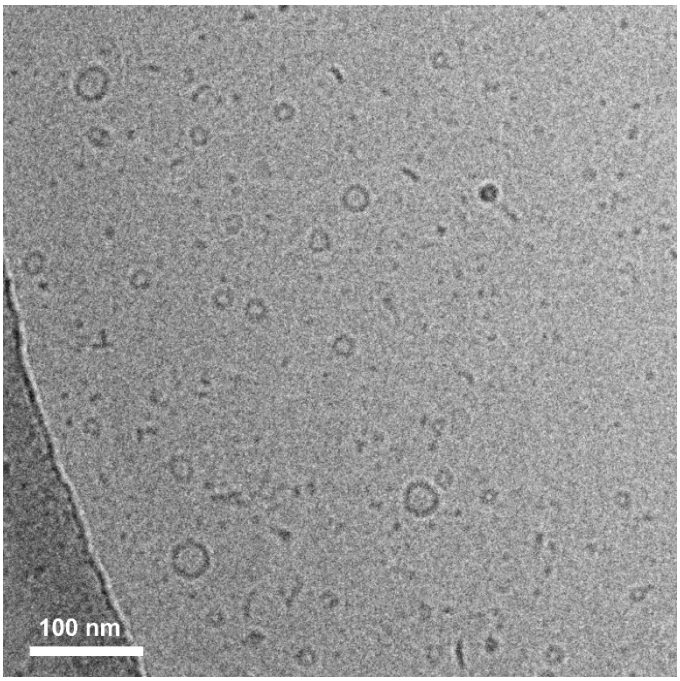

Fig. S17 Close-up cryo-TEM image of *trans*-**MBA** (7.0×10^{-3} M) in sodium borate buffer (pH = 9.3, 0.1 M) after irradiation with 312 nm for 10 min.

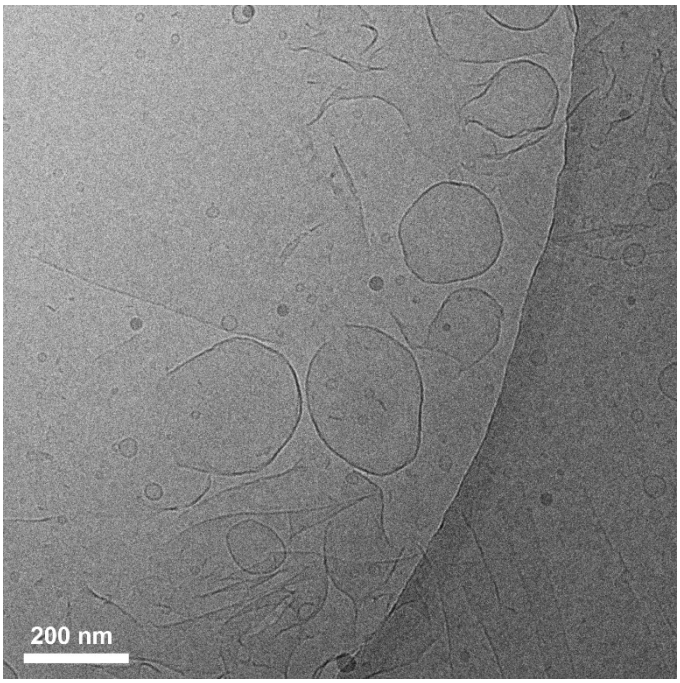

Fig. S18 Wide-field cryo-TEM image of *trans*-**MBA** (7.0×10^{-3} M) in sodium borate buffer (pH = 9.3, 0.1 M) after irradiation with 312 nm for 10 min and subsequent 365 nm irradiation for 10 min.

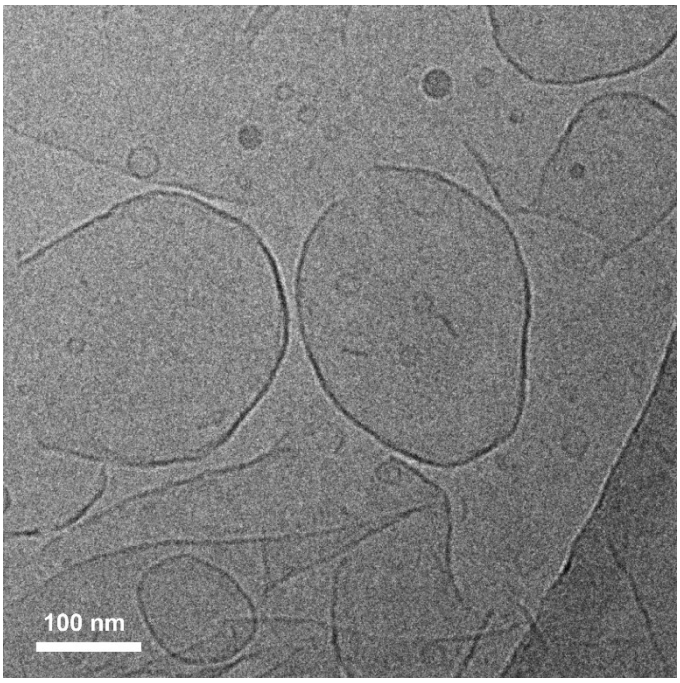

Fig. S19 Close-up cryo-TEM image of *trans*-**MBA** (7.0×10^{-3} M) in sodium borate buffer (pH = 9.3, 0.1 M) after irradiation with 312 nm for 10 min and subsequent 365 nm irradiation for 10 min.

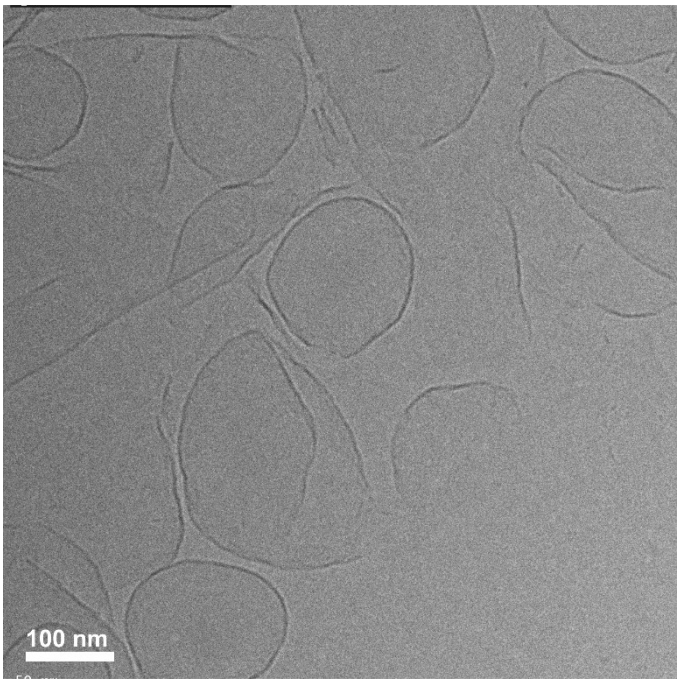

Fig. S20 Wide-field cryo-TEM image of *trans*-**MBA** (7.0×10^{-3} M) in sodium borate buffer (pH = 9.3, 0.1 M) after irradiation with 312 nm for 10 min and subsequent 365 nm irradiation for 10 min as well as a heating-cooling cycle.

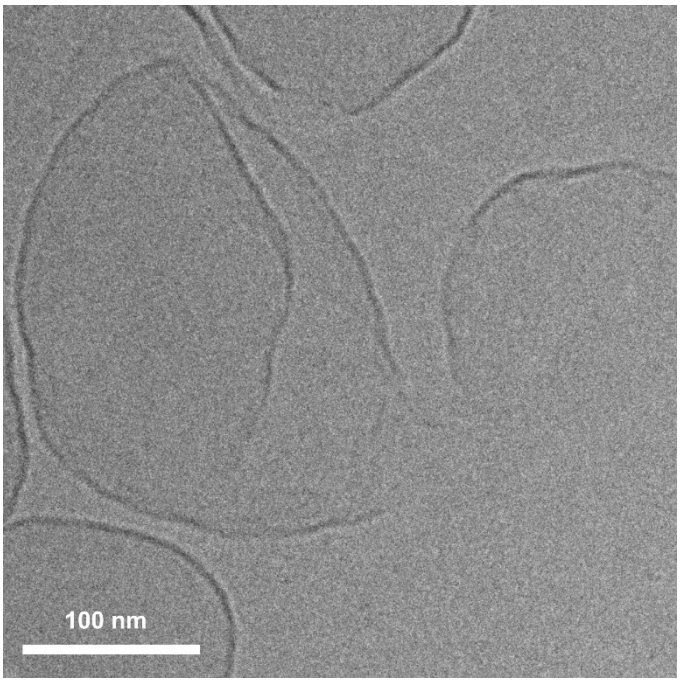

Fig. S21 Close-up cryo-TEM image of *trans*-**MBA** (7.0×10^{-3} M) in sodium borate buffer (pH = 9.3, 0.1 M) after irradiation with 312 nm for 10 min and subsequent 365 nm irradiation for 10 min as well as a heating-cooling cycle.

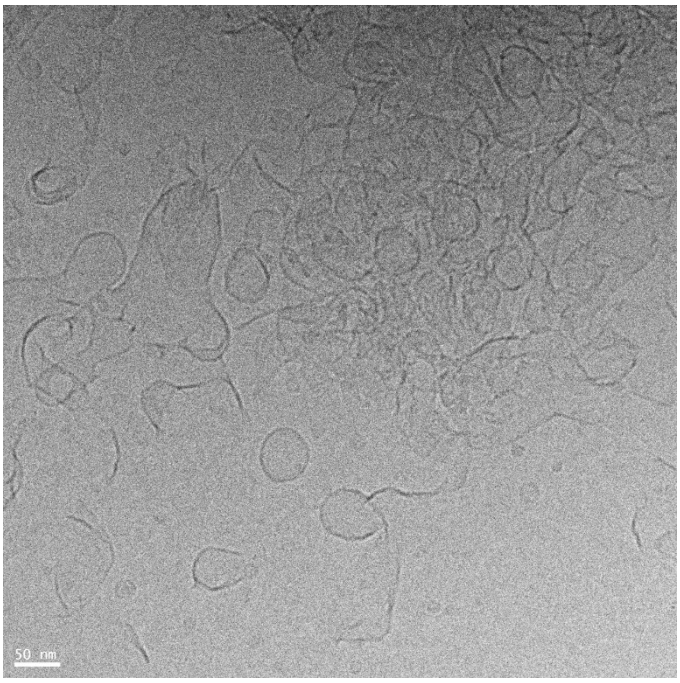

Fig. S22 Wide-field cryo-TEM image of *trans*-**MBA** (7.0×10^{-3} M) in aq. NaOH solution with pH = 8.8.

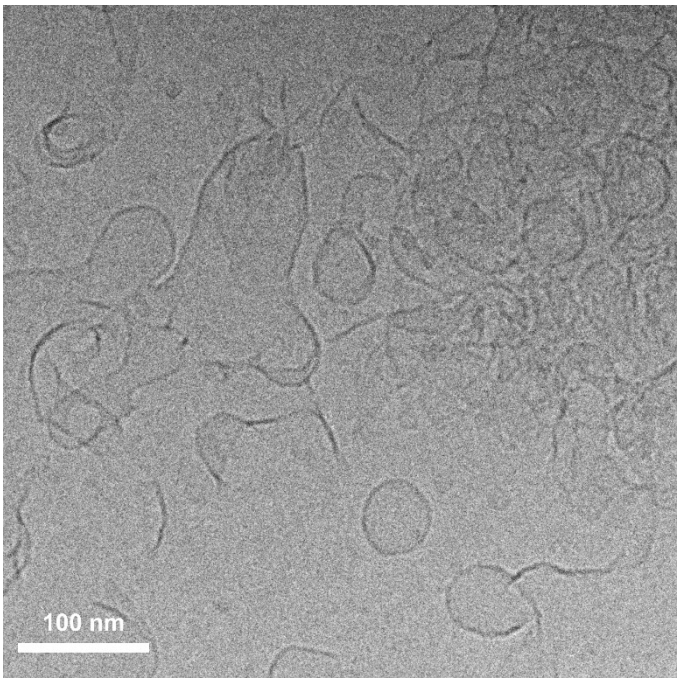

Fig. S23 Close-up cryo-TEM image of *trans*-**MBA** (7.0×10^{-3} M) in aq. NaOH solution with pH = 8.8.

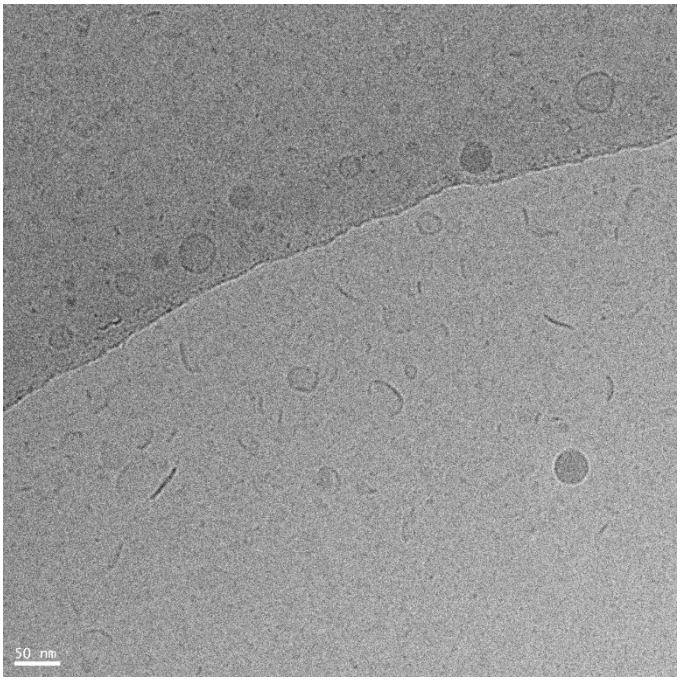

Fig. S24 Wide-field cryo-TEM image of *trans*-**MBA** (7.0×10^{-3} M) in aq. NaOH solution with pH = 9.8.

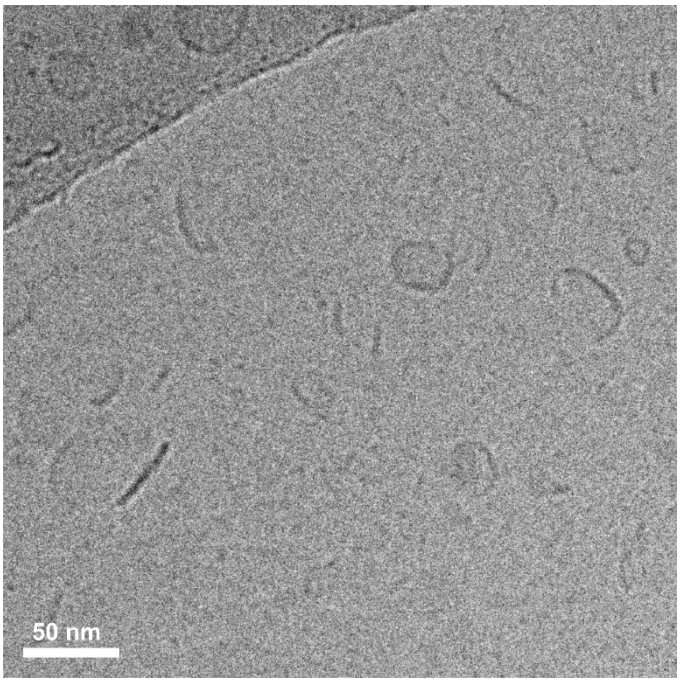

Fig. S25 Close-up cryo-TEM image of *trans*-**MBA** (7.0×10^{-3} M) in aq. NaOH solution with pH = 9.8.

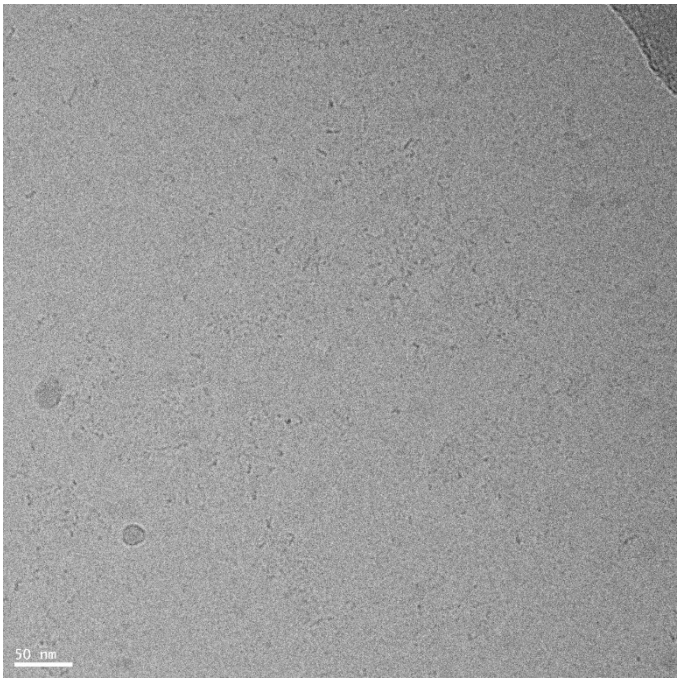

Fig. S26 Wide-field cryo-TEM image of *trans*-**MBA** (7.0×10^{-3} M) in aq. NaOH solution with pH = 11.

.

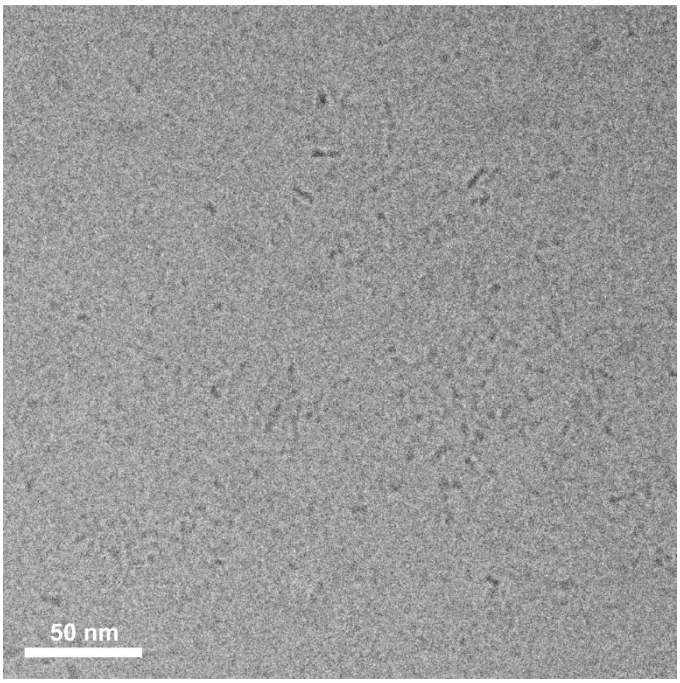

Fig. S27 Close-up cryo-TEM image of *trans*-**MBA** (7.0×10^{-3} M) in aq. NaOH solution with pH = 11.

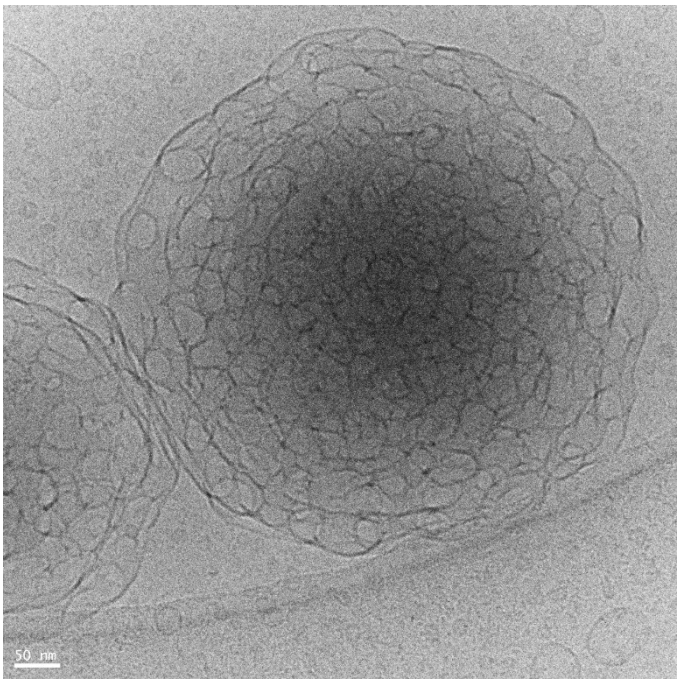

Fig. S28 Wide-field cryo-TEM image of *trans*-**MBA** (7.0×10^{-3} M) in aq. NaOH solution after adjusting its pH to 9.4 by adding an aq. HCl stock solution starting from pH 11.

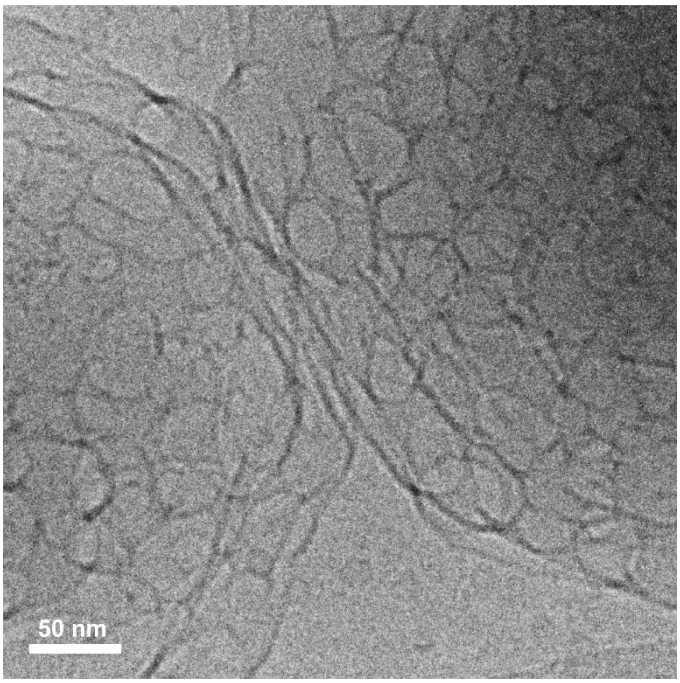

Fig. S29 Close-up cryo-TEM image of *trans*-**MBA** (7.0×10^{-3} M) in aq. NaOH solution after adjusting its pH to 9.4 by adding an aq. HCl stock solution starting from pH 11.

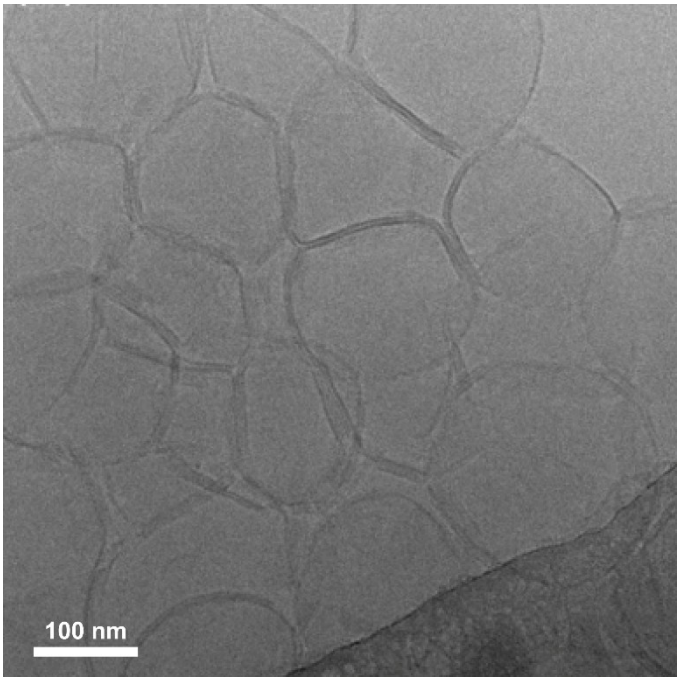

Fig. S30 Wide-field cryo-TEM images of *trans*-**MBA** carboxylates (7.0×10^{-3} M) in 0.1 M NaCl solution.

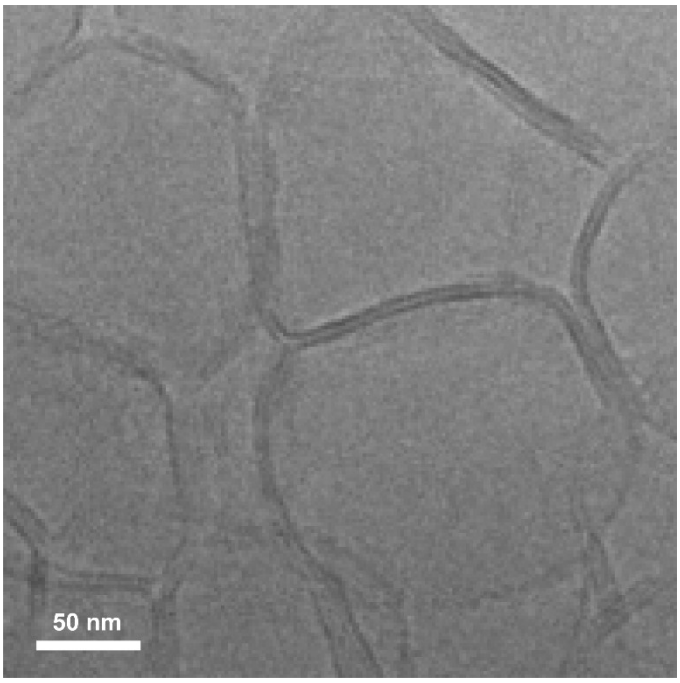

Fig. S31 Close-up cryo-TEM images of *trans*-**MBA** carboxylates (7.0×10^{-3} M) in 0.1 M NaCl solution.

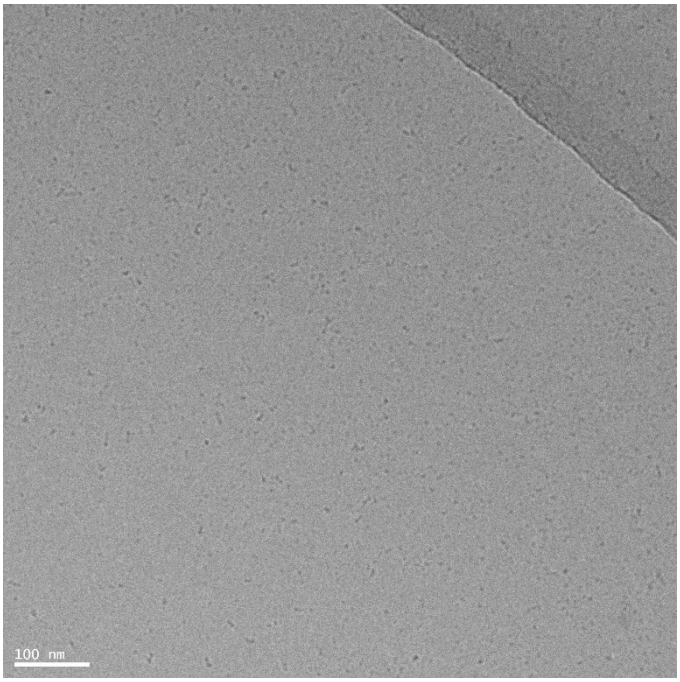

Fig. S32 Wide-field cryo-TEM image of stable *cis*-**MBA** (7.0×10^{-3} M) in sodium borate buffer.

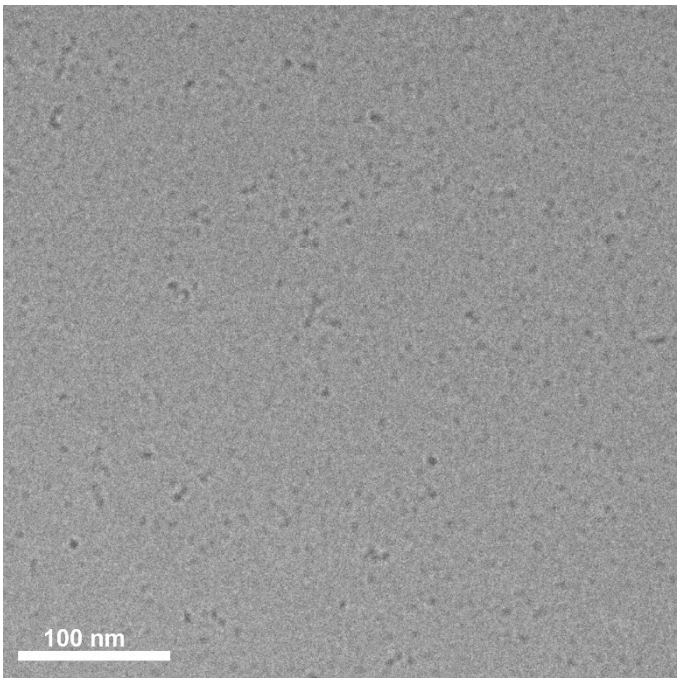

Fig. S33 Close-up cryo-TEM image of stable *cis*-**MBA** (7.0×10^{-3} M) in sodium borate buffer.

References

1 T. van Leeuwen, J. Gan, J. C. M. Kistemaker, S. F. Pizzolato, M. Chang and B. L. Feringa, *Chem. A Eur. J.*, 2016, **22**, 7054–7058.

2 T. M. Neubauer, T. van Leeuwen, D. Zhao, A. S. Lubbe, J. C. M. Kistemaker and B. L. Feringa, *Org. Lett.*, 2014, **16**, 4220–4223.

3 F. Tantakitti, J. Boekhoven, X. Wang, R. V. Kazantsev, T. Yu, J. Li, E. Zhuang, R. Zandi, J. H. Ortony, C. J. Newcomb, L. C. Palmer, G. S. Shekhawat, M. O. de la Cruz, G. C. Schatz and S. I. Stupp, *Nat. Mater.*, 2016, **15**, 469–476.

4 F. K. C. Leung, T. van den Enk, T. Kajitani, J. Chen, M. C. A. Stuart, J. Kuipers, T. Fukushima and B. L. Feringa, *J. Am. Chem. Soc.*, 2018, **140**, 17724−17733.

5 D. J. van Dijken, J. Chen, M. C. A. Stuart, L. Hou and B. L. Feringa, *J. Am. Chem. Soc.*, 2016, **138**, 660–669.